

Collective Instabilities in RHIC

M. Blaskiewicz

September 1994

Collider Accelerator Department
Brookhaven National Laboratory

U.S. Department of Energy

USDOE Office of Science (SC)

Notice: This technical note has been authored by employees of Brookhaven Science Associates, LLC under Contract No. DE-AC02-76CH00016 with the U.S. Department of Energy. The publisher by accepting the technical note for publication acknowledges that the United States Government retains a non-exclusive, paid-up, irrevocable, world-wide license to publish or reproduce the published form of this technical note, or allow others to do so, for United States Government purposes.

DISCLAIMER

This report was prepared as an account of work sponsored by an agency of the United States Government. Neither the United States Government nor any agency thereof, nor any of their employees, nor any of their contractors, subcontractors, or their employees, makes any warranty, express or implied, or assumes any legal liability or responsibility for the accuracy, completeness, or any third party's use or the results of such use of any information, apparatus, product, or process disclosed, or represents that its use would not infringe privately owned rights. Reference herein to any specific commercial product, process, or service by trade name, trademark, manufacturer, or otherwise, does not necessarily constitute or imply its endorsement, recommendation, or favoring by the United States Government or any agency thereof or its contractors or subcontractors. The views and opinions of authors expressed herein do not necessarily state or reflect those of the United States Government or any agency thereof.

Collective Instabilities in RHIC

Editors: S. Peggs & W.W. MacKay

Authors: M. Blaskiewicz, D.P. Deng, W.W. MacKay,
V. Mane, S. Peggs, A. Ratti, J. Rose, T. Shea, J. Wei

Revision 1.3
September 20, 1994

Contents

1	Introduction	1
1.1	The Relativistic Heavy Ion Collider	1
1.2	Machine cycle	1
1.2.1	Injection	2
1.2.2	Acceleration and transition	2
1.2.3	Rebucketing	3
1.2.4	Storage	3
1.3	Machine parameters	3
1.4	Nomenclature	8
1.4.1	Wake fields and impedances	8
1.5	RHIC impedance model	10
1.5.1	Devices not considered	11
2	Broadband Impedances	12
2.1	Overview	12
2.2	Simple inductive devices	13
2.3	Beampipe aperture transitions	13
2.4	Expansion bellows	14
2.5	Beampipe chamber wall impedance	15
2.6	Beam position monitors	16
2.7	Injection kickers	17
2.8	Gate valve	18
2.9	Vacuum ports	19
2.10	Beam collimators	19
2.11	Abort kickers	19
2.12	Total broadband impedance	22
3	RF cavity impedances	23
3.1	Introduction	23
3.2	Accelerating cavity impedances	24
3.2.1	Tuning range	25
3.2.2	HOM damper	26

3.3	Storage cavity impedances	27
3.3.1	Tuning range	28
4	Impedance database	30
5	Feedback and damping systems	32
5.1	Transverse system	32
5.2	Longitudinal system	33
6	Stability calculations	35
6.1	Longitudinal instabilities	35
6.1.1	The microwave instability	35
6.1.2	Longitudinal coupled bunch instability	37
6.2	Transverse instabilities	41
6.2.1	Weak coupling calculations	41
6.2.2	Calculations with mode coupling	44
6.3	Landau damping in RHIC	45
6.4	The head-tail instability	46
7	Summary and Comments	48

Chapter 1

Introduction

1.1 The Relativistic Heavy Ion Collider

This report summarizes the current knowledge of various collective effects which may lead to instabilities in the Relativistic Heavy Ion Collider, (RHIC). It updates the results of the March 1988 Workshop on the RHIC Performance[1]; however, even this document should be considered a progress report rather than a final report. Two areas which will not be covered by this report are intrabeam scattering, which has been covered elsewhere[2, 3], and beam-beam interactions, which fall into the category of single particle dynamics.

RHIC is designed to collide fully stripped ions from protons to gold, at a maximum energy of 250 GeV (protons) or 100 GeV/u (gold)[4]. Counter-rotating beams of particles will collide head-on at up to six interaction regions. The two intersecting superconducting rings, Blue and Yellow, have a circumference of 3.834 km that yields a maximum revolution frequency of $f_{rev} = 78.2$ kHz. Room temperature equipment is located in various warm regions of the rings. The rf system of RHIC consists of a set of 26 MHz cavities for injection and acceleration, and a set of 196 MHz cavities for storage[3].

Beams of protons and gold cover the extreme ends of the operating conditions; other ion beams should give results which fall somewhere in between.

1.2 Machine cycle

In general there are four phases to the machine cycle: injection, acceleration, “rebucketing”, and storage. Rebucketing occurs at top energy when beam is transferred from the 26 MHz rf buckets used for injection and acceleration, to the 196 MHz buckets used for storage. Machine cycles for protons and gold in RHIC will be quite different from each other in practice. For example, all ion species cross transition during the acceleration part of the cycle, when the

Lorentz factor $\gamma = \gamma_t = 22.89$, except for protons, which will be injected above transition[5, 6].

Vulnerability to instabilities is largest during injection, storage, and during transition crossing. For example, emittance blowup at transition is found to be a problem when RHIC is modeled by a constant $|Z/n|$ value of 1.5 Ω or more[5]. In reality, of course, the impedance of RHIC will be a much more complicated function of frequency.

A brief description of the four phases of the machine cycle follows. (A detailed discussion of the machine cycle may be found in Ref.[3].)

1.2.1 Injection

The injector system for RHIC consists of two linacs (one for protons, and one for other ions), the AGS Booster, and the AGS, as well as transport lines between the various machines. Between the AGS and the two rings of RHIC is the AGS-To-RHIC (ATR) transport line which splits symmetrically into two lines: one for each of the RHIC rings. Bunches are injected one at a time into RHIC, with a single bunch injected in one pulse into a bucket of the RHIC 26 MHz rf system. For identical species in both rings, successive AGS cycles alternate between filling Blue and Yellow rings. This is performed by reversing the current in a single switching dipole at the symmetric split of the transfer line. For nonidentical species (e. g., protons on gold) one ring will be filled before the other, since all of the injector system will have to be retuned for the second ion species.

The natural time scale for injection into RHIC is set by the AGS, which has an acceleration cycle time of three seconds. Up to 12 bunches of protons are accelerated in one batch during an AGS cycle, but for other ions there will be only 3 bunches per batch. It therefore takes 30 seconds to fill each ring with 57 bunches of protons, and 114 seconds for other ion species.

1.2.2 Acceleration and transition

Acceleration of the beams from injection to top energy is expected to take about 70 seconds. The limit is determined by the speed at which the superconducting magnets can be ramped from about 0.4 T to 3.5 T. For gold ions transition crossing occurs about 6.5 seconds into the acceleration ramp. RHIC will be the first superconducting accelerator to cross transition. It will also employ the first ever *linear bipolar* transition jump[7]. If there were no transition jump, then the effective time τ_J (Jøhnsen time) that it takes the beam to cross through transition would be about 140 ms. The γ_t -jump is designed to shift γ_t by $\Delta\gamma_t = -0.8$ in 60 ms; this should reduce τ_J by a factor of 8.3 to 17 ms. The remaining 60 seconds or so of acceleration occur after transition crossing.

Outside of transition crossing considerations, the study of the endpoints (injection and storage) should be satisfactory for understanding the limits of the

collective instabilities. Note that the rf cavities must be continuously retuned during acceleration, since the revolution frequency of the beam is increasing. As the cavities are retuned the higher order mode (HOM) frequencies may move around, possibly allowing some resonance to enhance an instability. As the actual cavities are tested, HOM dampers will be designed and tested to minimize this potential hazard. This is discussed in more detail below.

1.2.3 Rebucketing

After the beams have reached top energy, the rf systems are shifted from the acceleration mode (26 MHz) to the storage mode (196 MHz). Rather than using a slow adiabatic capture process, a bunch rotation is performed before capturing - rebucketing - a single bunch into a shorter bucket of the storage system.

First, the synchronous phase of the bunch is shifted, so that the bunch lies on an unstable fixed point of the 26 MHz system. The bunch is then allowed to elongate along the expanding lines of the separatrix for about 4 ms (300 turns). Then the synchronous phase is shifted back, so that the bunch once again lies on a 26 MHz stable fixed point, but is now mismatched. It is then allowed to rotate for about 3/8 of a synchrotron period (about 15 ms) so that the bunch is short in time, but tall in momentum spread. Finally, the 26 MHz system is abruptly turned off, and the 196 MHz system turned on, with a voltage that matches the beam ellipse. The whole process takes about 20 ms.

1.2.4 Storage

Storage times will vary from a few hours to about 10 hours. At the beginning of the storage, some of the interaction regions will be tuned for collisions by applying a “low beta squeeze”. This will reduce the collision point beta, β^* , from about 10 m to as little as 1 m, shrinking the transverse beam size and enhancing the luminosity. The process of reducing the interaction beam size is not expected to have an impact on the collective instabilities. Instead, the dominant multiparticle effect during storage is intrabeam scattering.

The machine cycle is summarized for protons in Table 1.1 and for gold ions in Table 1.2.

1.3 Machine parameters

RHIC parameters which are often referred to are gathered here together for convenience in Tables 1.3 through 1.7. They are used consistently throughout this report.

OPERATION	DURATION		
	Time [s]	Number of Turns	Synchrotron Periods
Injection (1 st bunch)	30	2×10^6	~ 2000
Acceleration	60	5×10^6	~ 3000
Rebucketing	0.020	1500	~ 1
Storage (10hr)	3.6×10^4	3×10^9	$\sim 10^7$

Table 1.1: Summary of proton machine cycle.

OPERATION	DURATION		
	Time [s]	Number of Turns	Synchrotron Periods
Injection (1 st bunch)	114	9×10^6	$\sim 10^4$
Acceleration($< \gamma_t$)	6.5	5×10^5	~ 500
Transition	0.017	1300	—
Acceleration($> \gamma_t$)	53	4×10^6	~ 2000
Rebucketing	0.020	1500	~ 1
Storage (10hr)	3.6×10^4	3×10^9	$\sim 10^7$

Table 1.2: Summary of gold machine cycle.

Name	Symbol	Value	Units
Circumference	C	3833.845	m
Average radius	R	610.1754	m
AGS circumference ratio	C_{ags}/C	4/19	
Revolution frequency ($v=c$)	f_{rev}	78.196	kHz
Revolution period ($v=c$)	T_{rev}	12.788	μs
Nominal number of bunches	N_b	57	
Upgrade		114	
Nominal bunch spacing	S_b	67.260	m
Upgrade		33.630	m
Nominal bunch time spacing ($v=c$)	T_b	224.4	ns
Upgrade		112.2	ns
Dipole bending radius	ρ	242.7806	m
Injection rigidity	$B\rho$	97.5	Tm
Top energy		839.5	Tm
Injection dipole field	B	.4016	T
Top energy		3.458	T
Transition Lorentz factor	γ_t	22.89	

Table 1.3: General RHIC machine parameters.

Name	Symbol	Value	Units
Acceleration harmonic number	h_{acc}	114x3 = 342	
Storage	h_{store}	114x22 = 2508	
Acceleration rf wavelength	λ_{acc}	11.2101	m
Storage	λ_{store}	1.5287	m
Acceleration rf frequency ($v=c$)	f_{acc}	26.743	MHz
Storage	f_{store}	196.116	MHz

Table 1.4: RHIC rf system general parameters.

Name	Symbol	Units	INJECTION	STORE
Nominal bunch intensity	N_b	10^9	100.0	100.0
Upgrade			250.0	250.0
Transverse emittance (95%)	ϵ_N	$\pi\mu\text{m}$	15	15
Bunch area (95%)	S	eV-s/u	.3	.3
rf voltage	V_{rf}	MV	.2	6.0
Synchrotron frequency	f_s	Hz	55.3	333.
RMS bunch length	σ_s	m	.353	.072
RMS momentum spread	σ_p/p	10^{-3}	.466	.265

Table 1.5: PROTONS: nominal beam parameters at various times.

Name	Symbol	Units	Injec -tion	Transi -tion	Start Store	End Store
Nominal bunch intensity	N_b	10^9	1.0	1.0	1.0	
Upgrade			2.0	2.0	2.0	
Transverse emittance (95%)	ϵ_N	$\pi\mu\text{m}$	10	15	15	40
Bunch area (95%)	S	eV-s/u	.2	.3	.4	1.2
rf voltage	V_{rf}	MV	.17	.30	6.00	6.00
Synchrotron frequency	f_s	Hz	121.	-	388.	388.
RMS bunch length	σ_s	m	.467	-	.119	.206
RMS momentum spread	σ_p/p	10^{-3}	.271	-	.529	.917

Table 1.6: GOLD: nominal beam parameters at various times.

Name	Units	Symbol	INJECTION	STORAGE
Horizontal betatron tune		Q_h	28.19	28.19
Vertical		Q_v	29.18	29.18
Horizontal chromaticity		χ_h	~ -3	~ 2
Vertical		χ_v	~ -3	~ 2
FODO cell length	m	L_{fodo}	29.658	
Horizontal cell phase advance	deg.	ϕ_h	80.7	81.2
Vertical	deg.	ϕ_v	85.5	86.4
Max horizontal FODO beta	m	$\beta_{h\ max}$	48.6	48.6
Min	m	$\beta_{h\ min}$	10.8	10.7
Max vertical FODO beta	m	$\beta_{v\ max}$	47.4	47.2
Min	m	$\beta_{v\ min}$	10.1	9.9
Max FODO dispersion	m	η_{max}	1.81	1.83
Min	m	η_{min}	.95	.92
Ringwide beta max in triplet	m	$\hat{\beta}$	145.6	1345.0
Interaction Point beta	m	β^*		
2, 4, 10, and 12 o'clock			10.0	10.0
6 and 8 o'clock			10.0	1.0

Table 1.7: RHIC lattice parameters.

1.4 Nomenclature

It is unfortunate, but not surprising, that various different sign and nomenclature conventions are found in the literature of wakefield, impedances and instabilities. This report adopts the conventions and nomenclature used in Chao's textbook[8], and tries to use them consistently throughout.

1.4.1 Wake fields and impedances

The interaction between the beam and its environment can lead to beam instabilities. As a charged bunch passes through a structure with conducting walls such as a beam pipe or rf cavity, eddy currents are formed in the walls. In the simplest case these eddy currents merely dissipate energy in the resistive walls; this dissipated energy comes, of course, from the energy of the beam itself. A more careful examination of the problem shows that there can be an interaction from the walls which may have a reactive component in addition to the resistance. It is useful to define a wake potential function and characterize the wall environment by frequency dependent impedances[9].

Consider a source particle moving down a beampipe with an offset a , and charge q . The charge and current may be decomposed in terms of multipole moments ρ_m and \vec{j}_m ,

$$\rho = \sum_{m=0}^{\infty} \rho_m \quad (1.1)$$

and

$$\vec{j} = \sum_{m=0}^{\infty} \vec{j}_m \quad (1.2)$$

where the moments are defined through

$$\rho_m = \frac{I_m}{\pi a^{m+1}(1 + \delta_{m0})} \delta(s - ct) \delta(r - a) \cos(m\theta) \quad (1.3)$$

and

$$\vec{j}_m = c\rho_m \hat{s} \quad (1.4)$$

Each moment corresponds to an infinitesimally thin ring with radius a and $\cos(m\theta)$ angular distribution, in a coordinate system where \hat{s} is a unit vector along the axis, r is the radial distance from the axis, and θ is an angle in the transverse plane. The current moment I_m is defined by

$$I_m = qa^m \quad \text{for } m \neq 0 \quad (1.5)$$

and

$$I_0 = q \quad (1.6)$$

Consider next a test particle of charge e following at a distance z behind the source particle, as they pass through an accelerator component of length L . The Lorentz force seen by the test charge is

$$\vec{F} = e \left(\vec{E} + \vec{v} \times \vec{B} \right) \quad (1.7)$$

where

$$\vec{v} = c \hat{s} \quad (1.8)$$

This force has longitudinal and transverse components F^{\parallel} and F^{\perp} given by

$$F^{\parallel} = e E_s \quad (1.9)$$

and

$$F^{\perp} = \hat{\theta} e (E_{\theta} + cB_r) + \hat{r} e (E_r + cB_{\theta}) \quad (1.10)$$

The net effect that one moment of the source charge has on the test particle is found by integration to be

$$\int_{-L/2}^{L/2} F^{\parallel} ds = -e I_m W'_m(z) r^m \cos(m\theta) \quad (1.11)$$

and

$$\int_{-L/2}^{L/2} F^{\perp} ds = -e I_m W_m(z) m r^m (\hat{r} \cos(m\theta) - \hat{\theta} \sin(m\theta)) \quad (1.12)$$

The integrals on the left hand side of these last two equations are called the “wake potentials”, while the function $W_m(z)$ that is introduced on the right hand side is called the “wake function”. Note that the longitudinal wake potential is proportional to $W'_m(z)$, the derivative of the wake function taken with respect to z .

The longitudinal and transverse impedances, Z_m^{\parallel} and Z_m^{\perp} , are given by the Fourier transform of $W'_m(z)$ and $W_m(z)$, respectively.

$$Z_m^{\parallel}(\omega) = \int_{-\infty}^{\infty} W'_m(z) e^{-i\omega z/c} \frac{dz}{c} \quad (1.13)$$

and

$$Z_m^{\perp}(\omega) = i \int_{-\infty}^{\infty} W_m(z) e^{-i\omega z/c} \frac{dz}{c} \quad (1.14)$$

Since attention mostly turns to $m = 0$ longitudinal effects and $m = 1$ transverse effects, it is common to talk about $Z^{\parallel} = Z_0^{\parallel}$ as the “longitudinal impedance”, and $Z^{\perp} = Z_1^{\perp}$ as the “transverse impedance”. Even more loosely, the longitudinal coupling impedance Z^{\parallel} is often referred to simply as Z , the “impedance”.

Lastly, it is also common to refer to the “broadband impedance” Z/n , which is properly defined as

$$\frac{Z}{n} = \frac{Z_0^{\parallel}(n 2\pi f_{rev})}{n} \quad (1.15)$$

where f_{rev} is the revolution frequency, and n is a harmonic of the revolution frequency. The broadband impedance has the advantage of being approximately constant in the low frequency limit, for many inductive accelerator components.

1.5 RHIC impedance model

An object resembling a closed cavity can support narrowband (high Q) resonances, and is naturally represented by a set of R , Q and ω_r values for those resonances, where

$$Z^{\parallel}(\omega) = \frac{R_{sh}}{1 + iQ \left[\frac{\omega_r}{\omega} - \frac{\omega}{\omega_r} \right]} \quad (1.16)$$

Here R_{sh} is the shunt impedance, Q is the quality factor and ω_r is the resonance frequency.

Conversely, an open ended device from which energy easily radiates is often represented by a single Z/n broadband value, implying that Z/n is approximately constant over the frequency range of interest, and that the impedance is inductive. The impedance function can be calculated analytically for some simple RHIC devices, with reasonable accuracy. It is calculated numerically for other, more complex devices, using MAFIA[10]. The impedances of broadband devices are calculated in the time domain, as the excited wake fields decay in a short time, while the impedances of narrowband devices are calculated in the frequency domain.

RF cavities dominate the narrow band impedance spectrum. In each ring of RHIC there is a pair of 26 MHz cavities for injection and acceleration. For storage there is a total of ten 196 MHz cavities in both rings; four of these are common to both rings, and the other six are distributed as separate triplets in each ring to give a effective total of seven storage cavities per ring.

Chapters 2 and 3, “Broadband impedances” and “RF cavity impedances”, describe the dominant features and devices in the beam environment that contribute significantly to broadband and narrowband parts of the RHIC impedance. The goal is to develop a “reasonably” accurate impedance model up to frequencies of 3 GHz, corresponding to the power spectrum of the shortest bunches expected in RHIC[11, 12]. This frequency is slightly less than the cutoff frequency of 3.32 GHz corresponding to the standard beampipe diameter of 6.91 cm. It is therefore not always strictly correct to assume that only the tails of broad resonances of common passive beampipe components are important.

The simple separation into general broadband devices and narrow band rf cavities is organizationally convenient, but is not so clear cut in practice. It is often difficult to say whether a particular object is broadband or narrowband.

1.5.1 Devices not considered

Some devices contribute to broad and narrow band impedances, but are not included in impedance estimates in this report, either because their contribution is negligibly small, or because they are still being studied as work in progress. They include:

1. Y-shaped beam chamber near the DX dipole splitting magnets. A detailed design is not yet available for this piece. There are 12 of these.
2. Injection Lambertson septum, with Y-shaped chamber, one per ring. The design is complete, but analysis has not yet begun. It is not expected to play a significant role.
3. Abort kickers and sweepers, and associated vacuum chambers. Design work is in progress for the kickers and sweepers, which will have a significant impedance contribution. See the section on “Abort kickers”, below, for more discussion.
4. The PHOBOS experiment vacuum chamber. This vacuum chamber has constrictions for short detectors close to the beam, that cause it to have a cavity like appearance. Design iterations are currently in progress, in discussions with the experimental collaboration, to minimize potential problems.
5. The vacuum pipe curvature, which makes a negligible impedance contribution[13]

With the possible exception of the fast abort kickers, none of these devices is expected to make a significant change in the total impedance of RHIC, nor to change the conclusions of this report.

It should be reiterated that this report does not pretend to present a cut-and-dried analysis, but is a living work in progress. Revisions of this report will be released, at timely intervals, as knowledge of RHIC improves.

Chapter 2

Broadband Impedances

2.1 Overview

RHIC is a superconducting collider, and so the individual vacuum chambers shrink and expand a great deal during cool down and warm up. An important consequence is that there are a large number of vacuum bellows in each ring that have the potential to dominate the broadband impedance of RHIC if they are not shielded. The vacuum chamber itself carries a impedance, even when it is smooth and featureless. Warm and cold parts of the chamber contribute separately to the net wall impedance.

While arc dipoles and quadrupoles have a coil ID of 8 cm, the Interaction Region (IR) quadrupoles have a coil ID of 13 cm. The cold circular beam pipe in the regular arcs that comprise most of the RHIC circumference has an ID of 6.911 cm, while the ID of the IR quad vacuum chamber is 12.28 cm. A tapered piece of vacuum chamber is located on either side of every IR, to make the transition between the two different pipe sizes. This piece is often referred to as a “warm-to-cold” transition, since the vacuum pipe makes a simultaneous transition from cryogenic to room temperatures. It is a simple and common example of the numerous major and minor aperture transitions that occur in the IRs, many of which are individually tailored to the needs of a particular IR, and all of which contribute to the broadband impedance. At the rare end of the spectrum is the special case of the vacuum chamber in the PHOBOS experiment that has several short constrictions and contributes to both broadband and narrowband impedances.

Beam position monitors are also present in relatively large numbers, with an impedance that is related to the sensitivity with which they detect beam. Vacuum gate valves and vacuum ports are quite numerous, but contribute only modestly to the total broadband impedance, and negligibly to the narrowband impedance, so long as they are properly shielded. Beam scrapers (or collimators)

are also present in small numbers, with a minor contribution to the broadband impedance, but a potentially significant narrowband contribution, if they are not appropriately shielded. The injection and abort kickers have a significant contribution to the total impedance.

2.2 Simple inductive devices

Small vacuum chamber discontinuities in RHIC, such as aperture transitions and expansion bellows, are normally inductive. If the bunch length obeys the relationship $\sigma \geq d/4$, where d is the beampipe diameter, then little of its power spectrum ($\leq 9\%$) is above the cutoff frequency of the vacuum chamber[14]. The beam leaves little energy behind when it passes by, since the beampipe will not support free waves below cutoff. The head of the beam will lose energy to the discontinuity, which can influence the tail. Above transition, the voltage induced when a bunch passes by an inductive object has a slope opposite in sign to the rf system wave slope. It tends to lengthen the bunch.

Simple expressions for the inductive impedance of common elements in RHIC are surprisingly accurate. For example, if the radius of the beampipe increases from r_1 to r_2 by an amount $\Delta \ll r_1$ in an aperture transition with a flare half-angle of θ ,

$$\frac{Z}{n} = -iZ_0 \frac{3}{2C} \left(\frac{r_1 \Delta^2}{r_2^2} \right) \left(\frac{2\theta}{\pi} \right)^{1/2} \quad (2.1)$$

where C is the circumference and $Z_0 = 377 \Omega$ is the free space impedance[14]. Similarly, a vacuum bellows with a total of N small rectangular corrugations, each of length g and depth Δ , on a beampipe of nominal radius r , has an approximate impedance of

$$\frac{Z}{n} = -iZ_0 \frac{N}{C} \left(\frac{g\Delta}{r} \right) \quad (2.2)$$

A numerical investigation has shown that these expressions are accurate at the 20% level for common RHIC components, up to frequencies of 1.5 GHz[15].

2.3 Beampipe aperture transitions

The most significant aperture changes occur at the warm-to-cold transitions near Q4 quadrupoles on either side of each IR, where the ID of the vacuum pipe increases from 6.91 cm to 12.28 cm. There are other warm-to-cold transitions (for example next to every Q3 triplet quadrupole) that are not accompanied by aperture transitions.

Instead of making an abrupt step between two beam pipes of different radii, it is desirable to make the aperture transition near Q4 more graceful by using

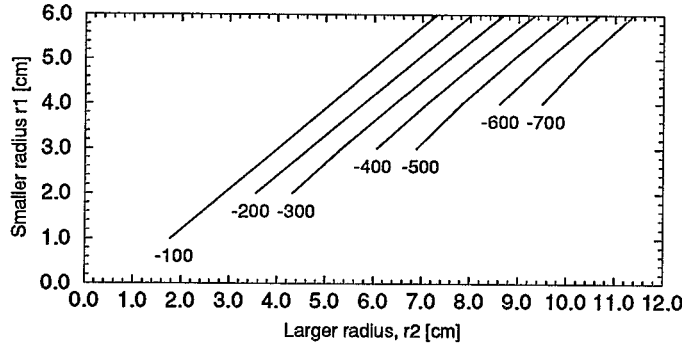


Figure 2.1: Contours of constant Z/n [$i\mu\Omega$], for a RHIC aperture transition with a five-to-one flare.

a tapered conical section of beam pipe. Eq. 2.1 shows that the impedance is significantly reduced if the aperture transition occurs gradually. A warm-to-cold transition with a taper length of 13.4 cm, 5 times as long as the difference in pipe radii, illustrates the “five-to-one” rule that is applied to RHIC aperture transitions, wherever possible. Figure 2.1 shows predicted contours of constant $\text{Im}(Z/n)$ in the space of the beam pipe radii, when the five-to-one rule is applied.

Figure 2.2 shows the imaginary part of the impedance of the warm to cold transition, as calculated by the numerical code MAFIA[10]. The impedance is adequately described by the Z/n value of $-0.35 i m\Omega$ predicted by Equation 2.1 and Figure 2.1. Since there are 16 such transitions in RHIC (including those surrounding injection and abort kickers), they contribute only about $-0.006 i \Omega$ to the total broadband Z/n .

2.4 Expansion bellows

RHIC has approximately one vacuum bellows per magnet, to allow for thermal expansion and contraction. The most common are the 428 cold bellows with an ID of 6.91 cm, and the 72 warm bellows with an ID of 12.28 cm. There are 30(40) corrugations of depth 0.94(1.27) cm and length 0.25(0.32) cm in the common cold(warm) bellows. The parameters of one set of bellows are its total length l , number of corrugations N , depth of the corrugation Δ and beam pipe radius b . Unshielded bellows show a broad resonance at a frequency that is a strong function of the depth of the corrugation.

Unshielded 6.91 cm diameter bellows with $\Delta = 1\text{cm}$, $l = 15\text{cm}$ and $N = 30$ show a resonance at 4.7 GHz with $R = 850 \Omega$, $Q = 7$, while unshielded 12.28 cm diameter bellows with $\Delta = 1\text{cm}$, $l = 15\text{cm}$ and $N = 30$ display a resonance

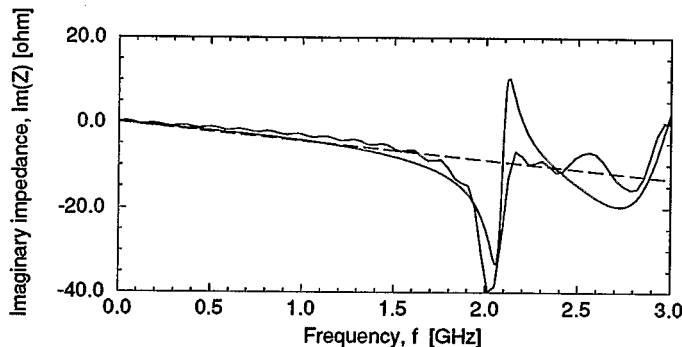


Figure 2.2: Impedance of a RHIC warm to cold transition. The complex curve is a numerical calculation, the smooth curve is a two resonance fit, and the dashed straight line is $Z/n = -0.35 i m\Omega$.

at 3.6 GHz, with $R = 170 \Omega$ and $Q = 2.5$. These resonance frequencies are above the pipe cutoff of 3.3 GHz, leaving a large inductance below 3 GHz that is reasonably well modeled by the broadband expression of Equation 2.2.

The common RHIC bellows alone would contribute a broadband impedance of $Z/n = -1.01 i \Omega$ if left unshielded, an unacceptably large value[16]. Consequently, all of the common bellows (except 10 warm ones) will be shielded, although some of the rarer specialized bellows will be left unshielded. The unshielded bellows impedance function measured on the bench using a wire method is in good agreement with calculations[17]. The estimated total impedance of all common RHIC bellows, with shielding, is only about $Z/n = -0.02 i \Omega$.

2.5 Beampipe chamber wall impedance

The “resistive wall” impedance of the cylindrical vacuum chamber is given for all but the highest and lowest frequencies by

$$Z^{\parallel}(f) = (1 - i) \sum (L/\pi d \sigma \delta) \quad (2.3)$$

where L is the length of a section of beampipe with an inner diameter of d , and σ is the conductivity[8, 18]. The skin depth δ is given by

$$\delta = \sqrt{(1/\mu_0 \sigma \pi f)} \quad (2.4)$$

with μ_0 the permeability of free space. The resistive wall impedance varies like the square root of the frequency, and so it dominates the low frequency end of the impedance spectrum.

Inner Diameter [cm]	Temperature	Conductivity [1/Ω.m]	Length [km]
6.91	cold	2×10^6	2.955
12.28	warm	1×10^6	0.879

Table 2.1: Vacuum pipe parameters in a simple two pipe model of the resistive wall impedance.

A sum over different sections of beam pipe is included in Equation 2.3 because the conductivity of the stainless steel vacuum pipe varies by a factor of two between cold and warm regions, and the aperture of the pipe varies considerably, especially in the interaction regions. Nonetheless, a naive but reasonably accurate representation of the total resistive wall impedance is found by considering RHIC to consist of two pipes, with the parameters listed in Table 2.1. This “two pipe model” yields a total resistive wall contribution of

$$Z^{\parallel}(f) = (1 - i) f^{1/2} [\text{GHz}^{1/2}] 748 \Omega \quad (2.5)$$

2.6 Beam position monitors

The most common RHIC stripline beam position monitor (BPM) works in only one plane, and so has two strips. Its impedance is directly related to its sensitivity, with a periodic form given by[19]

$$Z^{\parallel}(\omega) = 2Z_0 \left(\frac{\phi_0}{2\pi}\right)^2 \left[\sin^2\left(\frac{\omega l}{c}\right) - i \sin\left(\frac{\omega l}{c}\right) \cos\left(\frac{\omega l}{c}\right) \right] \quad (2.6)$$

where $l = 23$ cm is the strip length, $\phi_0 = 80^\circ$ is the angle each strip subtends, and $Z_0 = 50 \Omega$ is the characteristic impedance of the BPM. The amplitude of this impedance is 4.93Ω , with a period, $c/2l$, of 0.65 GHz. There are 174 single plane BPMs in each ring, as well as 72 dual plane BPMs that have four strips, and twice the impedance of Equation 2.6. Adding the contribution of all these BPMs together results, in the low frequency limit, in an inductive contribution to the total impedance of

$$Z^{\parallel}/n \simeq -0.58 i [\Omega] \quad \text{for } f \ll 0.65 [\text{GHz}] \quad (2.7)$$

In the high frequency limit the envelope of Z/n drops off like

$$|Z^{\parallel}/n| \leq \frac{0.12}{f[\text{GHz}]} [\Omega] \quad \text{for } f \gg 0.65 [\text{GHz}] \quad (2.8)$$

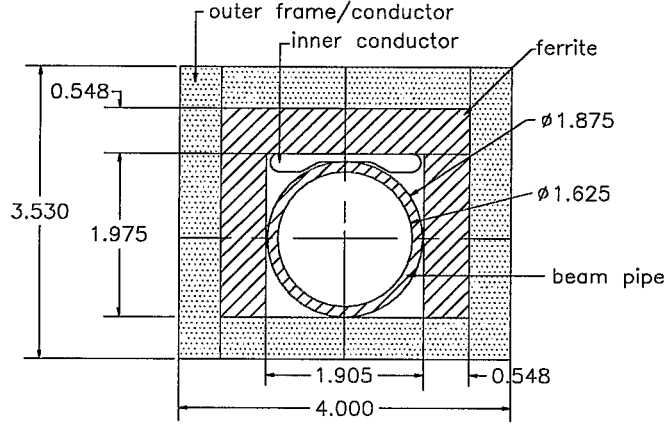


Figure 2.3: RHIC injection kicker cross section

2.7 Injection kickers

The injection kicker is a pulsed transmission line kicker, with alternate ferrite and ceramic sections[20]. The total length of each kicker module is $l = 1.1$ m and there are $N = 4$ such units in each ring. Figure 2.3 shows a cross section of the magnet, with C-shaped ferrite, an inner conductor and an outer conductor. At the time of writing, a prototype module recently became available for bench impedance measurements. The nominal beam vacuum chamber is made of ceramic with an aperture of 41.3 mm. The ceramic chamber allows the fast rising magnetic fields to penetrate the walls. It also allows a strong coupling of the beam and the magnet. The low frequency impedance amplitude is estimated to be[21]

$$\frac{Z}{n} = \frac{Z_0 N}{4n} \left\{ \left[1 - \cos \left(2\pi \frac{f}{f_0} \right) \right] - i \left[2\pi \frac{f}{f_0} - \sin \left(2\pi \frac{f}{f_0} \right) \right] \right\} \quad (2.9)$$

where $Z_0 = 25 \Omega$ is the characteristic impedance of the kicker. The characteristic frequency f_0 is given by

$$f_0 = \frac{Z_0 w}{\mu_0 h l} \simeq 18 \text{ MHz} \quad (2.10)$$

where $h = w = 2.38$ cm is the kicker half height and width.

The approximation given in Equation 2.9 is only valid at low frequencies, $f \leq 50$ MHz. It is difficult to calculate the impedance of the magnet at higher frequencies, as the magnetic properties of the ferrite depend on the frequency,

and ferrites are lossy at high frequencies. A preliminary wire measurement of the kicker module gives a rough estimate of the total broadband impedance contribution from all four modules as $|Z/n| \simeq 0.1 \Omega$ at 750 MHz. This is about as much as the impedance from all the other devices in the machine put together. Therefore, two methods of reducing the coupling impedance are currently under investigation - a metallic coating on the vacuum chamber, and noninductive metallic strips.

The nominal current rise time in the kicker is 30 nsec. If the vacuum chamber includes a thin round conductive surface of radius $b = 2.1$ cm, thickness d and conductivity σ , the risetime due to shielding by eddy currents is given by[22]

$$\tau_e = \frac{\mu_0 \sigma b d}{2} \quad (2.11)$$

For example, a $d = 4 \mu\text{m}$ thick coating of a material such as stainless steel, with $\sigma = 10^6 [1/\Omega\cdot\text{m}]$, will give a minimum kicker risetime of $\tau_e = 26$ nsec. The effect that this coating has on the beam is parameterised by the frequency at which the skin depth is equal to the coating thickness. This ‘‘critical skin depth frequency’’ is given by

$$f_{skin} = \frac{1}{\pi \mu_0 \sigma d^2} \quad (2.12)$$

A $4 \mu\text{m}$ stainless steel coating gives a critical frequency $f_{skin} = 16$ GHz. This does not help the beam coupling impedance, as all the beam frequencies up to 16 GHz will penetrate the conductive coating. A coating material with suitably low conductivity (such as stainless steel) is desirable, since the eddy current risetime is proportional to (σd) and is held fixed, while the skin depth frequency is proportional to $1/(\sigma d^2)$.

A second possibility is to lay two copper metal strips along the length of the magnet, in a noninductive fashion on the top and bottom of the vacuum chamber. Each strip might have a thickness of, say, 0.5 mm, and a width of 0.5 cm. Only very small eddy currents are induced in the strips by the fast rise of the kicker fields. However, the strips will only be partially effective in reducing the coupling between the beam and the magnet. The effect of such strips on the beam impedance has yet to be determined from bench measurements, while the effect of the strips on the shape of the kicker field is being investigated numerically with MAFIA. Preliminary results suggest that the magnetic field of the kicker is slightly distorted near the strips, but is not affected in most of the region inside the beampipe.

2.8 Gate valve

There are about 40 gate valves in each ring. These will be shielded, in order to avoid narrowband resonances.

2.9 Vacuum ports

About half of the expansion bellows in the arcs have an associated vacuum pump out port, in the form of a cylindrical pipe intersecting the beampipe at right angles to make a “T”. In most cases the side pipe ID is 2.2 cm and the beampipe ID is 6.91 cm. Because the side pipe is relatively narrow, very little wake field penetrates into it, and the associated impedance is very small. The net effect of all 233 such ports, left unshielded, is a $|Z/n|$ value of less than $0.002\ \Omega$. There are also 16 similar ports at the warm to cold transitions. However, it is necessary to shield the approximately 36 ports per ring where the side pipe ID is about 12 cm and the beampipe ID is 12.28 cm. A rectangular wire mesh with a coarse spacing of 3 cm placed over the end of the side pipe removes essentially all of the impedance contribution of these warm vacuum ports, while causing a negligible loss in the pumping conductance[23].

2.10 Beam collimators

There are 4 beam collimators in each ring. They consist of a transversely movable section, connected to the beam pipe on each side with a bellows, as shown in Figure 2.4. The collimator itself is an “L” shaped piece of metal mounted inside a rectangular vacuum box. Since the space between the collimator and the vacuum chamber has the potential to act like a cavity, with significant narrowband behavior, the collimator will be shielded. Image currents will flow smoothly from one side of the vacuum box to the other, without seeing significant discontinuities. Details of this shielding design are currently under development, and will incorporate impedance minimizing design features.

2.11 Abort kickers

There are 7 abort kicker magnet modules in each ring. Five of them are ferrite loaded fast risetime elements which move the beam onto the internal dump. The remaining 2 modules are slower elements used to sweep the beam across the dump face to minimize instantaneous energy deposition. These sweeper magnets will be constructed using tape wound cores. There is no detailed design available yet on these elements though they will need ceramic beam pipes and thus are “similar” to the injection kickers at a superficial level. The physical aperture of these elements will be larger than the injection kickers due to the location in the ring and thus can be expected to have a somewhat lower impedance.

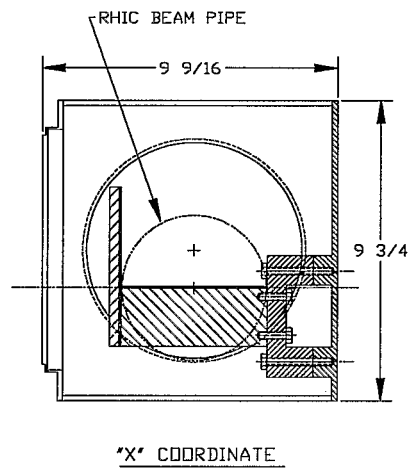
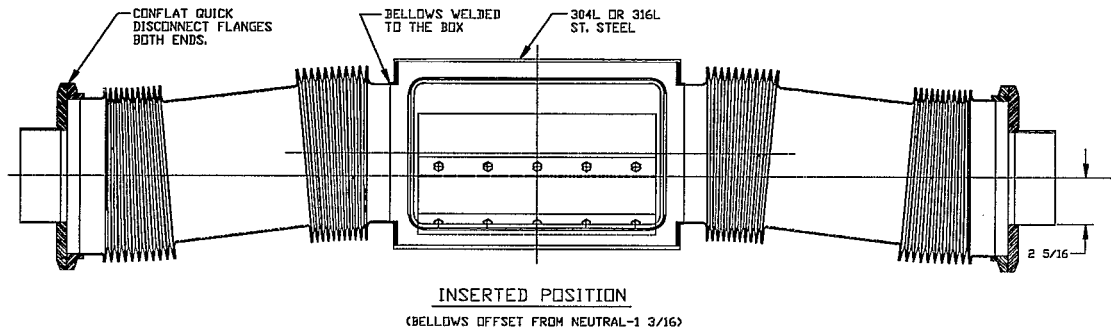


Figure 2.4: RHIC collimators.

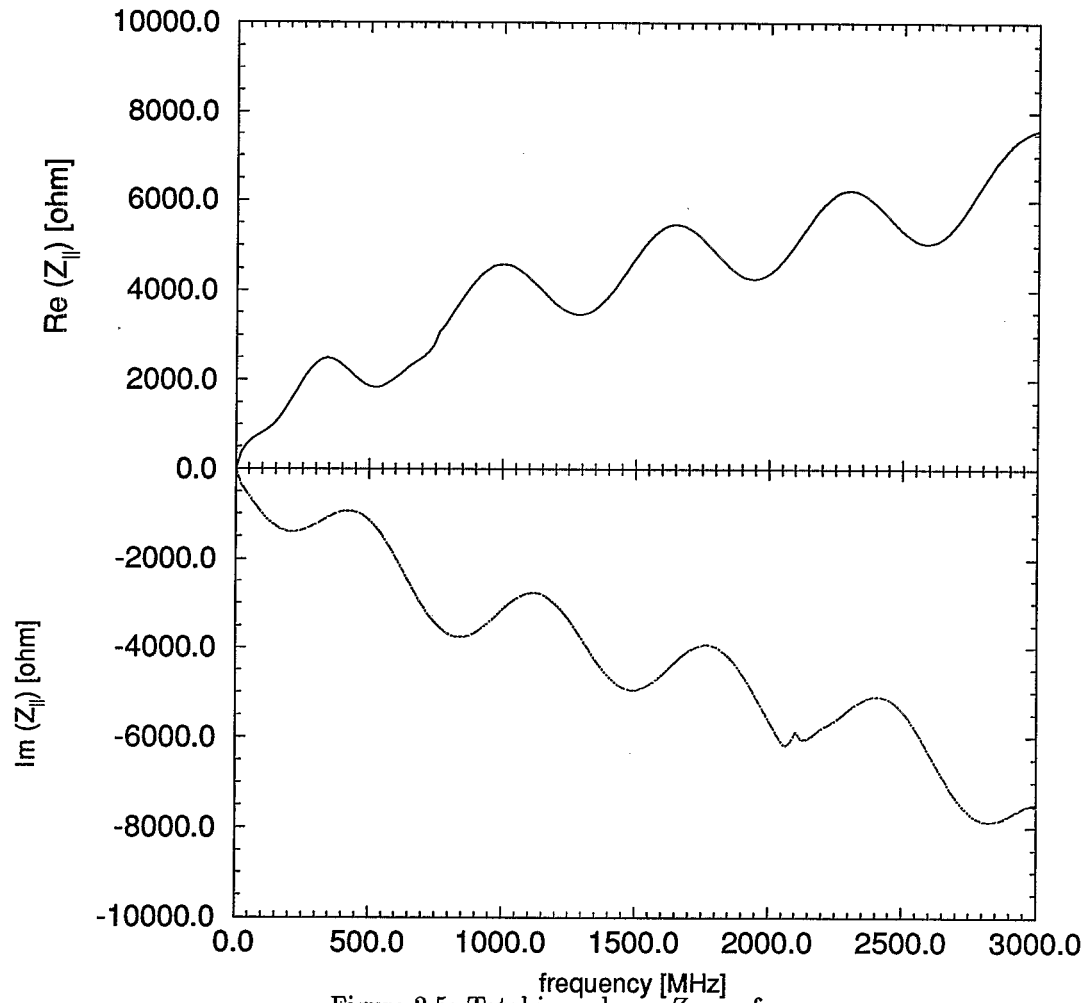


Figure 2.5: Total impedance $Z_{||}$ vs. frequency.

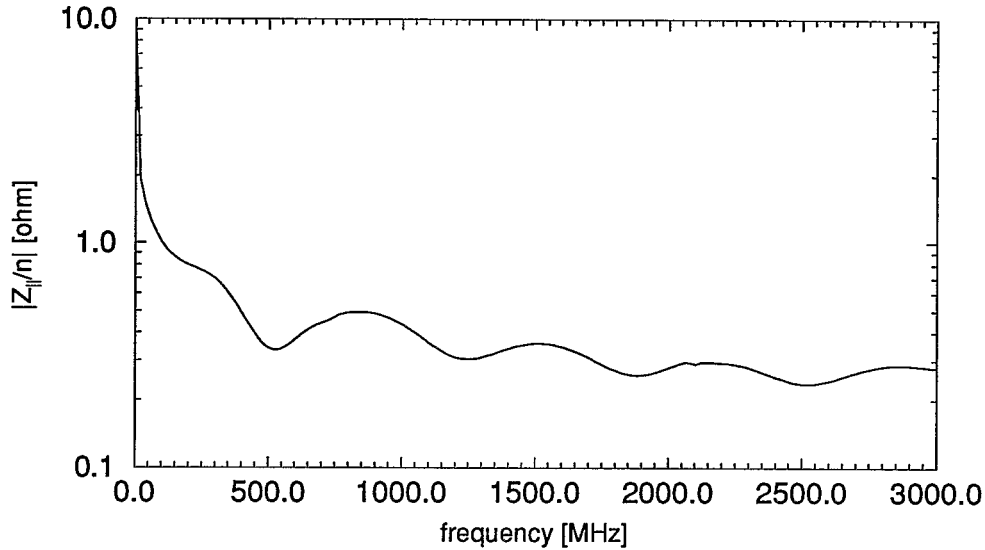


Figure 2.6: Total $|Z_{||}/n|$ vs. frequency.

2.12 Total broadband impedance

The impedance from the above mentioned devices is summed up in Fig. 2.5, which plots the total RHIC broadband impedance vs. frequency, up to 3 GHz. The total impedance includes contributions from beam pipe resistive wall, 246 beam position monitors, 285 vacuum ports, approximately 500 bellows, 16 warm to cold transitions, 4 injection kicker modules and 7 abort kicker modules. The impedance of the injection kicker is extrapolated up to 3 GHz, beyond the maximum measurement frequency of 1 GHz, using a resistive wall fit. The abort kickers are conservatively assumed to make a contribution identical to the injection kickers.

Fig. 2.6 gives a plot of total $|Z/n|$ up to 3 GHz. At very low frequencies, up to about 100 MHz, main contribution is from beam chamber wall impedance and beam position monitors. At high frequencies the impedance falls off to about .25 ohm. At frequencies up to 1.5 GHz, the main contribution is from the kickers. Above 1.5 GHz, most of the above mentioned devices also make a contribution.

Chapter 3

RF cavity impedances

3.1 Introduction

The rf system must be capable of capturing, accelerating, and storing for 10 hours the nominal load of 57 bunches of particles with an average current of up to 70 mA. Three subsystems will be used:

1. An accelerating system to capture the injected bunches, accelerate through transition, and shorten the bunches at top energy. It operates at harmonic number 342, and uses a 26.7 MHz cavity developed by the RHIC rf group.
2. A storage system which accepts the shortened bunches at top energy and provides sufficient longitudinal focusing to keep the bunches short during the 10 hour colliding mode in the presence of intrabeam scattering. It operates at a harmonic number of 2508, and uses the well documented CERN SPS 200 MHz cavity tuned to 196.1 MHz for operation in RHIC[24].
3. A wideband system which operates on a bunch to bunch basis to damp injection momentum errors. It is also available to damp longitudinal coupled bunch instabilities.

Of these three systems, the accelerating and storage systems have narrow band cavities with high shunt impedances which contribute to coupled bunch instabilities, requiring the design of passive higher order mode (HOM) dampers to de-Q the high Q resonances. The wideband system is described in Chapter 5, "Feedback and damping systems".

Longitudinal and transverse impedance calculations have been performed for fundamental and higher order modes in both the accelerating and storage cavities. The wideband longitudinal kickers have not yet been designed, but they

will not contribute much to the machine impedance since there is only one per ring and they are inherently low Q devices. The narrow band impedances have been calculated using the codes MAFIA, SUPERFISH, and URMEL[10, 25, 26]. These codes calculate the longitudinal shunt impedance as

$$R_{sh} = \frac{[\text{Re}(\int E_z(z)e^{ikz/\beta} dz)]^2}{2P} \quad (3.1)$$

where P is the power dissipated in the cavity, E_z is the longitudinal electric field either on axis (monopole modes) or displaced at a radial offset of a (dipole, quadrupole modes, et cetera), k is the wave number (ω/c) and β is the ratio of the beam velocity to that of light.

The cavities also have transverse (dipole) modes which can couple strongly to the beam. The transverse shunt impedance of a cavity is given by the integral of the force acting on the beam, as

$$Z^\perp = -i \frac{\int_0^L (\vec{E} + \vec{v} \times \vec{B})_\perp ds}{\beta I a} \quad (3.2)$$

where L is the cavity length, I is the average bunch current, and a is the offset of the beam from the cavity axis. The beam must couple energy into the higher order transverse modes through the electric field and hence there is a relation between the longitudinal and transverse shunt impedances. This is given (broadband) for right circular cylinders as

$$Z_1^\perp = \frac{2c}{b^2} \frac{Z_0^\parallel}{\omega} \quad (3.3)$$

where b is the beampipe radius.

This chapter records shunt impedances, quality factors and frequencies of the higher order modes in the two main rf systems. Cavity impedances for the RHIC cavities have been calculated and successfully compared with bead perturbation measurements of R/Q for selected modes. These impedances are used in Chapter 6, "Stability calculations", to calculate longitudinal coupled-bunch growth rates using both the storage ring code ZAP and analytical methods. The two methods are found to be in excellent agreement.

3.2 Accelerating cavity impedances

There are two accelerating cavities in each ring, ultimately capable of providing up to 400 kV per cavity. Particle tracking studies[27] show that beams with a longitudinal emittance as high as 0.6 eV-sec/u can be rebucketed if the accelerating system voltage is 300 kV per cavity. Modest changes have been made to the original cavity geometry to make this possible, and have been implemented in the prototype cavity now undergoing bench tests.

The accelerating cavities consist of capacitively loaded quarter-wave structures with a close-coupled tetrode amplifier to minimize the time delay when local feedback is implemented. The ferrite tuner that was present in an earlier prototype design[27] has been replaced by a mechanical tuner. This has had the effect of raising the first HOM frequency from 64 MHz to 103 MHz. The higher order mode impedances were calculated with the codes SUPERFISH[25] and URMEL[26]. Bead perturbation measurements confirmed the calculated R/Q of the fundamental and will be used to measure HOMs, especially dipole modes as a function of asymmetries in the cavities, such as the power amplifier. The frequencies, shunt-impedances and Q 's for the longitudinal and transverse modes are given in Tables 3.1 and 3.2.

f_{rf} [MHz]	R_{sh} [M Ω]	Q	R/Q [Ω]
26.7	0.950	15750	60
103.3	0.129	26880	4.8
192.3	0.077	33430	2.3
276.5	0.174	28850	6.0
328.8	0.307	23260	13.2
394.2	0.156	45160	3.5

Table 3.1: Longitudinal modes of the 26.7 MHz accelerating cavity

3.2.1 Tuning range

The frequency tuning range required to compensate the change in ion velocity is dominated by the need to accelerate gold ions from $\gamma = 12.2$ to $\gamma = 108.4$. This results in a fundamental frequency of 26.6537 MHz at injection and 26.7426 MHz at top energy. Protons at top energy ($\gamma = 268.2$) require a slightly higher upper frequency of 26.7435 MHz. The mechanical tuner that shifts the fundamental over a range of approximately 90 kHz will also affect the frequencies of all higher order modes. Table 3.3 characterizes several longitudinal (i.e. monopole) modes as the cavities are tuned across the design frequency range. Some modes are tuned over tens of MHz and therefore will cross hundreds of beam rotation harmonics.

The cavities will change temperature during normal operation, and as a result, so will the frequencies of their modes. A worst case analysis of thermal detuning shows a 2 kHz/ $^{\circ}$ C shift of the fundamental frequency. This would be automatically corrected by the tuner, but the higher order modes will be tuned

f_{rf} [MHz]	R_t [Ω/m]	Q [10^4]	R/Q [Ω/m]
200.0	363	5.23	0.01
255.9	3416	4.55	0.07
309.6	2.880	2.32	–
348.1	30560	3.67	0.83
421.3	31860	5.06	0.63
479.9	75790	2.86	2.65
522.4	27360	5.40	0.51
550.5	2508	5.14	–
564.5	15700	4.85	0.32
587.9	18380	4.88	0.38
601.3	31	6.24	–
617.8	635	6.20	–
626.1	2983	6.48	–
660.3	2907	7.16	–
704.4	53680	7.38	0.73

Table 3.2: Transverse (dipole) modes of the 26.7 MHz accelerating cavity

over several rotation lines.

3.2.2 HOM damper

The broadband loop-coupled dampers on the 26.7 MHz cavity are placed so as to maximize the coupling to the few dangerous modes identified in the instability studies. Once a limit is placed on the impedance of the offending mode the required coupling can be easily determined. It is expected that most of the higher order modes from each cavity will fall in such a way that they will neither add nor subtract, because they will not have exactly the same frequency, due to mechanical imprecision. This is especially true of the highest frequency modes. Thus their R/Q values are not to be added, but rather are to be considered as two independent modes with very similar R/Q and f_{rf} values. Only the fundamental 26.7 MHz modes will add, through the use of the tuner and the beam control system.

For all of these reasons, it is practically impossible to identify and isolate a small number of particularly dangerous higher order modes before real experience with beam is gained. Therefore, the accelerating cavities will be equipped with a broadband HOM damper to reduce the Q of the modes for all tuner po-

f_{rf} [MHz] Tuner IN	f_{rf} [MHz] Tuner OUT	$\frac{R}{Q}$ [Ω] Tuner IN	$\frac{R}{Q}$ [Ω] Tuner OUT
26.65	26.74	67.0	67.0
103.34	103.45	4.80	4.83
192.11	192.29	2.31	2.47
276.32	277.27	6.03	5.48
328.60	331.66	13.3	13.1
394.13	395.32	3.43	3.66
479.10	481.40	4.93	4.06
519.35	516.83	2.19	5.22
525.51	535.03	na	3.76
560.40	551.22	0.26	0.40

Table 3.3: Resonant frequencies and strengths of longitudinal TM modes in 26 MHz cavities, versus the position of the mechanical tuner.

sitions. Prototype broadband HOM dampers have been constructed and tested, although the design has not yet been finalized. They are of the lumped LC notch type to reject the fundamental but allow a broad passband for higher order modes, which are then terminated. Cavity tests are about to begin.

The shunt impedances and Q 's listed in the tables are theoretical, undamped values. The ratio of shunt impedance and Q , (R/Q), is a property of the cavity geometry and is unchanged by mode dampers, which act to reduce both R and Q . It is reasonable to expect that an overall reduction of 15 to 25 dB will be achieved on specific problem modes.

3.3 Storage cavity impedances

The storage system consists of ten surplus CERN SPS cavities, the so-called SWC cavities, which are tuned from the SPS frequency of 200.1 MHz to 196.1 MHz for operation in RHIC. There are 4 cavities common to both rings in the four o'clock interaction region, and 3 additional cavities in each individual ring, for an effective 7 cavities per ring. Each cavity is capable of 1 MV of accelerating voltage for a total of 7 MV per ring. The cavities are tuned to the new frequency by deforming them with a large lead screw device which decreases the gap dimension from 294.5 mm to 271.8 mm. This lowers the fundamental mode frequency through an increase in the capacitance, and also changes the HOM frequencies.

f_{rf} [MHz]	R_{sh} [M Ω]	Q	R/Q [Ω]
196.1	*8.4	*49260	170
308.4	.0528	4400	12
445.0	.0084	1200	7
543.1	.0297	690	43
604.5	.0195	1500	13
844.5	.0010	1000	1
993.4	.0458	9900	4.6

Table 3.4: Longitudinal modes of the 196.1 MHz storage cavity. The frequency is from an URMEL calculation with the new geometry, while the R_{sh} and Q values are from CERN data (* = undamped).

The cavities have the original CERN HOM suppressors which consist of a quarter wave band reject notch filter to reject the fundamental and terminate the HOM's in 50 ohms. Since the narrowband reject filters are originally tuned to 200.1 MHz, they are modified for operation at 196 MHz. Because the passband is very broad and the coupling coefficient for HOM's depends on the spatial characteristics of the model fields, the damping effectiveness is expected to remain the same after the HOM damper is tuned to the RHIC frequency. The change in fundamental frequency therefore results in negligible change to the shunt impedance and Q of the HOM's, or to their spatial field variations.

The undamped cavity with the new gap geometry is modeled with URMEL to reproduce the new fundamental frequency, and to obtain the new HOM frequencies. These new URMEL HOM frequencies, combined with the damped shunt impedances reported from CERN[24, 28], are shown in Table 3.4. Dipole modes of the 196 MHz cavities are given in Table 3.5.

3.3.1 Tuning range

The storage cavities must be able to operate from $\gamma = 31.2$, during injection of protons, to $\gamma = 268.2$, at the top energy for protons. This results in a frequency range of 196.02 MHz to 196.12 MHz. In addition, the beam loading detuning requires -5.2 kHz for a total tuning range of 105 kHz, between full current at injection and zero current at top energy. This is well within the 400 kHz tuning range of the storage cavities.

f [MHz]	R_t/Q [Ω/m]	Q
394	18	1800
515	3	2500
526	6	2100
579	2	820
681	13	2000
716	1	3100
759	1	780

Table 3.5: Transverse (dipole) modes of the 196.1 MHz storage cavity. Frequencies are calculated values for cavity tuned to 196 MHz, shunt impedance and Q are measured values with dampers from CERN 200 MHz configuration.

Chapter 4

Impedance database

Aperture and impedance information are maintained in tables in the *beam-pipe* relational database, using the *SYBASE* database management system [11, 29]. This database contains an inventory of the geometries and impedances of significant RHIC devices, so that an accurate impedance and aperture model may be readily obtained.

Each ring is divided into contiguous lattice slots. A “slot” is a complete assembly that is the smallest unit which can be installed in (or replaced or removed from) the tunnel. For example, arc dipoles and CQS packages (Corrector Quad Sextupole) are slots. The longitudinal s coordinate at the beginning of a slot corresponds to the s coordinate of the end of the previous slot. The connection between the non-unique *lattice_name* of a lattice slot, and the unique *SiteWide-Name* of an accelerator object is contained in the *ap_list* table. Also, each lattice slot is described by a *genericslot*. The table *ap_list* gives the *genericslot* for a given lattice slot, its coordinate s and the machine (Blue or Yellow).

The *genericslots* are further divided into *segments* and this information is contained in the *ap_slotsegment* table. Each segment is characterised by its length, beginning cross section and end cross section, recorded in the *ap_segcs* table. The shape and dimensions for each cross section, called *acsname*, are maintained in *ap_cross_section* table. In the case at hand there is no significant change of aperture within a segment.

The machine aperture can be reconstructed, as a function of the longitudinal coordinate s , by inspecting the lattice slot, *genericslot* and segment information.

Geometry parameters vary from segment to segment. For example, unshielded bellows are described by the depth of corrugation, length of corrugations, and the pipe aperture, while vacuum ports are described by port radius, port length and the beam pipe radius. The segments are so chosen that they fall into a given category of *geometry_type* for impedance calculations. The *seginfo* table gives the *geometry_type* for a given segment.

The impedance of a simple object such as resistive wall beampipe, or a

beam position monitor, is given by a straightforward analytical expression such as Equation 2.3 or Equation 2.6. The impedance of a complex object, such as a bellows or a vacuum port, must be determined numerically, even though approximate expressions may be valid in the low frequency limit. In this case a numerical description is fitted by an appropriate curve, and the fitting parameters are stored in one or more database tables. For a given *geometry_type*, the *impedance_info* table gives the names of all tables which contain its impedance. Examples of impedance tables are *resonance*, *linear_impedance*, *bpm_impedance* and *wall_impedance*.

As an example, the beam chamber at the 2 o'clock IR near the PHOBOS detector consists of six pillbox-like cavities. For each cavity such as "phobos_1", the *seginfo* table points to the *geometry_type* *phobos*, and the *impedance_info* table points to the *impedance_table* *resonance*. PHOBOS data in the *resonance* table are calculated using the eigenmode solver in MAFIA[10]. All resonant segments have entries in the *resonance* table. Some segments, such as an accelerating cavity, have no entries anywhere else but there. All resonances of a given segment are recorded, up to 3 GHz.

The program SEGCOUNT is designed to read all the tables, count segments, and check for referential integrity. For all the lattice slots in a ring, it finds the corresponding *genericslot* and adds up the total number of each *genericslot*. For each *genericslot*, it finds the segments and counts them. Hence the *quantity* of each *segname* in a ring is obtained. The impedance contributions from all of these segments are added up and an impedance model of the machine is obtained.

Chapter 5

Feedback and damping systems

5.1 Transverse system

The transverse system will employ stripline kickers which produce both electric and magnetic deflection and can support a wide system bandwidth. They will be used in conjunction with beam position monitors located in regions of low dispersion to control injection errors, to excite coherent betatron oscillations in order to measure the tune, and to suppress coherent transverse coupled bunch instabilities. Power amplifiers will have a bandwidth sufficient to allow operation on each bunch individually, and will provide enough power to cope with the expected injection errors. The power requirement of the system is driven by the damping rate needed to recover from these injection errors. In order to estimate this power, the following case is considered.

The maximum allowed injection errors will lead to betatron oscillations with an amplitude of 2 mm. To avoid emittance dilution of the beam, a damping time equivalent to 100 revolutions or 1.3 ms is required. In order to decrease the damping time for injection errors, the gain will be programmed so that the maximum kick is applied every turn as long as the oscillation amplitude is above some predetermined value. Once the minimum amplitude is reached an amplitude dependent damping program is reinstated in order to suppress any potential instability. The angular kick per turn, θ , needed to provide the above damping time is $0.4\mu\text{radian}$ per turn. For relativistic ions, the kicker and power amplifier requirements are determined through the relation

$$\theta = \frac{rZeVl}{Ad\gamma m_0 c^2} \quad (5.1)$$

where Ze is the charge state, A the atomic mass number, m_0 the specific mass

of a nucleon, d and l are respectively the separation and length of the stripline pair, and V is the voltage of a stripline relative to the beam pipe. For gold this gives $VL \simeq 100$ Vm. If the striplines are 2m long, and the impedance R is 50Ω , the total power requirement per plane should be about

$$P = \frac{(2V)^2}{2R} \simeq 400 \text{ W} \quad (5.2)$$

Transverse head-tail modes could be damped, if necessary, with only a minimal cost increase to the system. The basic hardware (pickups, cables, amplifiers, and kickers) will have a 200 MHz bandwidth. At injection the proton bunches are about 6.5 ns long (95%), and gold bunches are about 16 ns long, so there should be plenty of bandwidth to handle transverse head-tail modes. Although the feedback circuits of the present design are not designed for this bandwidth, diagnosis of the head-tail modes can be made. Additionally, transfer functions could be measured by exciting a mode with a kicker while measuring the resultant amplitude with a pickup.

5.2 Longitudinal system

Longitudinal emittance blowup can occur during injection when a bunch injected off-center in a bucket starts a dipole oscillation. The particle distribution in the bucket filaments, due to synchrotron frequency spread within the bunch. RHIC has a tight longitudinal emittance budget and so needs a longitudinal damper at injection to correct injection errors from the AGS, and to control rigid coupled bunch instabilities.

The bunches in each AGS batch are transferred into the RHIC rings one by one. Phase errors from injection can be kept small, since they mainly come from the momentum differences between the two machines. These momentum errors fluctuate from batch to batch, demanding bunch-by-bunch correction. In the upgrade scenario of 114 bunches in a RHIC ring, the beam frequency is 8.9 MHz. The bandwidth of the damper system will be at least this large, and will be centered at the frequency of the rf acceleration cavities, 26.7 MHz.

The acceptable uncorrected injection momentum error is 10^{-5} for negligible longitudinal emittance blowup. However, it is quite possible that the errors will be as large as 10^{-4} , which, if uncorrected, would lead to a 30% blowup for a 0.2eVs/u gold beam. This higher limit sets a goal for the damping system.

The correction signal is derived by detecting the phase error of a bunch center relative to the center of its rf bucket. The phase error is converted to a momentum correction by shifting the signal 90° in synchrotron phase to produce a voltage kick which is applied by the damper cavity. The damping rate of synchrotron oscillations depends on the voltage kick; the higher the damping rate required, the higher the voltage, which costs more. The choice of the voltage is a compromise between the two competing factors of economy

and efficiency. Simulations show that the damping time is approximately 5τ , or 0.05 s at 1 kV per kick, and the resultant emittance blowup at the end of damping is only 5%.

The power requirement is $P = V^2/2R$, where R is the impedance. For $V = 1$ kV and $R = 50 \Omega$, $P = 10$ kW. The contribution of the damper system to the broadband longitudinal coupling impedance is negligible.

Chapter 6

Stability calculations

6.1 Longitudinal instabilities

6.1.1 The microwave instability

Beam-induced fields with wavelengths short compared to the bunch length may induce microwave instabilities in a single bunch. For a specified beam intensity, this phenomenon imposes a limit on the longitudinal impedance, $|Z^{\parallel}/n|$, within the frequency range from the average bunch-spectrum frequency of, typically, 400 MHz to the beampipe cut-off frequency of about 3.3 GHz. Above this limit, the natural synchrotron frequency spread is not sufficient to suppress an infinitesimal coherent perturbation in the longitudinal phase space distribution of the beam. For a bunched beam of peak current \hat{I} and rms momentum spread $\Delta p/p$, the threshold impedance [30, 31] is approximately given by

$$\left| \frac{Z^{\parallel}}{n} \right|_{th} = \frac{2\pi\beta^2 E |\eta| (\Delta p/p)^2}{Ze\hat{I}}, \quad (6.1)$$

where $E = Am_0c^2\gamma$ is the total energy, η is the phase slip factor, βc is the velocity, and Ze is the charge of the ion. Eq. 6.1 can also be expressed in terms of the number of particles N_0 per bunch and the rms bunch length σ_{ϕ} in rf phase,

$$\left| \frac{Z^{\parallel}}{n} \right|_{th} = \frac{\sqrt{2\pi} V_{rf} |\cos \phi_s| \sigma_{\phi}^3}{h^2 N_0 Ze \omega_0}, \quad (6.2)$$

where ω_0 is the revolution frequency, V_{rf} is the rf voltage, h is the harmonic number, and ϕ_s is the synchronous phase. At a given energy, the bunch is more stable with higher rf voltage V_{rf} which provides more frequency spread and Landau damping.

The proton beam is injected above the transition energy with a 95% longitudinal emittance (bunch area) of $S = 0.3$ eV·s. The growth in emittance

during acceleration is expected to be small. At top energy, the proton bunches are directly rebucketed with the 196 MHz storage rf system. With the nominal intensity of 10^{11} protons per bunch, the bunch area grows due to intrabeam scattering from 0.3 eV·s to about 0.7 eV·s during the 10 hour storage. Table 6.1 lists the threshold longitudinal impedance, corresponding to this intensity at various stages in the proton machine cycle.

	$ Z^{\parallel}/n _{th}$ [Ω]	S [eV·s]	V_{rf} [MV]	h
Injection	5.4	0.3	0.2	342
Top Energy	2.1	0.3	0.3	342
Rebucketing	2.1	0.3	0.3	342
Storage (start)	7.4	0.3	6.0	2508
(end)	26	0.7	6.0	2508

Table 6.1: Impedance threshold for microwave stability of proton bunches.

The gold beam is injected below transition using a matched rf voltage with a nominal bunch area of $S = 0.2$ eV·s/u and a nominal intensity of 10^9 ions per bunch. Due to intrabeam scattering at injection, the bunch area increases to about 0.3 eV·s/u just before transition crossing. Both the microwave instability and self-field mismatch may occur during transition crossing. In the presence of the γ_t -jump, the microwave threshold impedance is about 2.4 Ω , while the limit for a 10% area growth due to self-field mismatch is about 1.5 Ω [5]. After having reached the top energy, the gold bunches are then rebucketed by employing a bunch lengthening and rotation using the unstable fixed point. The gold bunch grows significantly during the 10 hour storage, due to intrabeam scattering. Longitudinally, particles will fill up the entire rf bucket of area 1.2 eV·s/u within the first hour. Table 6.2 lists the threshold longitudinal impedance at various stages in the gold machine cycle, using these parameters.

According to Tables 6.1 and 6.2, microwave instabilities are of no concern during the storage period. The lowest threshold for the proton beam occurs at the end of the acceleration, and for the gold beam at transition. In both cases, the average bunch-spectrum frequency is about 400 MHz and the threshold $|Z^{\parallel}/n|$ value is above 2 Ω . On the other hand, the machine broadband impedance $|Z^{\parallel}/n|$, positively inductive and resistive within the frequency range of interest, is estimated in section 2.12 to be less than 0.5 Ω for frequencies above 250 MHz. The space-charge broadband impedance, negatively inductive, is about 1.3 Ω at transition and is negligible at the top energy. RHIC is therefore expected to be stable against longitudinal microwave instabilities during

	$ Z^{\parallel}/n _{th}$ [Ω]	S [eV·s/u]	V_{rf} [MV]	h
Injection	47	0.2	0.17	342
Transition	2.4, 1.5*	0.3	0.3	342
Top Energy	16	0.4	0.3	342
Rebucketing	10	0.4	0.3	342
Storage (start)	55	0.4	6.0	2508
(end)	190	1	6.0	2508

Table 6.2: Impedance threshold for microwave stability of gold bunches.

the entire machine cycle.

6.1.2 Longitudinal coupled bunch instability

Longitudinal coupled bunch instability growth rates are calculated analytically and compared with the results obtained by the code ZAP[32]. It is assumed that the dominant impedances are the higher order modes of the rf cavities, as reported above in Chapter 3. Since the Fourier spectrum of the relatively long RHIC bunches falls off rapidly at higher frequencies, the calculation concentrates on the first few higher order modes of the cavity.

The worst case is used to calculate the growth rates, in which the cavity modes fall directly on synchrotron sidebands of the revolution lines. This is justified for a large circumference collider such as RHIC, where the separation of revolution lines is only 78 kHz. The cavity modes are very likely to cross the lines slowly, as the cavity is tuned with increasing beam-loading, and will certainly cross as the cavity is tuned to keep up with the change in velocity of the beam during acceleration. The modes will also drift with temperature. Although the tuning loop will keep the fundamental corrected for thermal detuning, the HOM's will still be affected. Our calculational precision is worse than the 78 kHz revolution line spacing, especially in the presence of the cavity amplifier, vacuum ports, et cetera. Accurate knowledge of the HOM frequencies, R_{SH} and Q awaits measurements of the actual cavities.

Growth rates are calculated for proton and gold beams at three places in the cycle: at injection, close to transition, and at the beginning of storage at top energy. It is found that the proton beam at injection is the most sensitive. This is the case analyzed below. The bunch parameters at injection are a bunch length of 6 ns (95%), a momentum spread of $\Delta p/p = 10^{-3}$, a synchrotron frequency of 45 Hz, 10^{11} particles per bunch, and 57 bunches. The code ZAP is

HOM Frequency [MHz]	rigid mode A	ZAP τ^{-1} [sec ⁻¹]	Nondegenerate τ^{-1} [sec ⁻¹]	Degenerate τ^{-1} [sec ⁻¹]
103	1	11.3	12	13.9
	2	5.0	3.76	5.1
192	1	9.9	2.5	3.25
	2	0.9	4.47	5.75
276	1	2.1	0.23	3.2
	2	0.9	0.005	6.3
329	1	35	0	4.6
	2	13.5	1.3	7.4

Table 6.3: Longitudinal multibunch growth rates for rigid dipole (A=1) and quadrupole (A=2) modes induced by undamped accelerating cavity higher order modes.

used with the Zotter formalism for parabolic bunches to find growth rates for each of the first few modes separately, shifting the input mode frequency to lie on the nearest synchrotron sideband. Parabolic bunches are used since they more accurately describe observed bunches in proton machines, while maintaining ease of analysis. Results are shown in Table 6.3 for the rigid dipole and quadrupole modes.

For the analytical approach the expression by Baartman[33] was used:

$$\frac{1}{\tau} = \frac{\omega_\phi}{r_\phi} \frac{I_0 R_{sh}}{V_T \cos(\phi_T)} F_m, \quad (6.3)$$

where ω_ϕ is the angular synchrotron frequency, r_ϕ is the bunch half length measured in radians of f_{rf} , I_0 is the dc beam current, R_{sh} the shunt impedance of the m^{th} cavity mode, and $V_T \cos(\phi_T)$ is the total rf voltage seen by the beam. The form factor F_m is given by [34]

$$F_m = m\mu(\mu+1) \left(\frac{2}{\chi}\right)^{2\mu+1} \frac{(m+2k+\mu)\Gamma(k+\mu)\Gamma(m+k+\mu)}{k!(m+k)!} J_{m+k+\mu}^2(\chi), \quad (6.4)$$

where $\chi = \omega_{res} t_\phi$ is the angular HOM frequency times the bunch half length in seconds. F_m is between 0 and 0.6 and is inversely proportional to ω_{rf} and

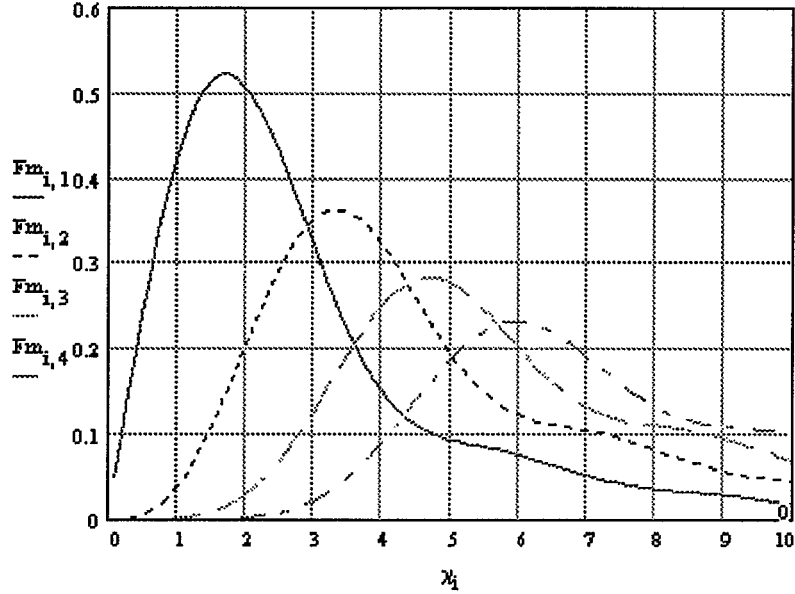


Figure 6.1: Form factors for degenerate case, radial modes summed for dipole (1), quadrupole (2), sextupole (3) and octupole (4).

the square of the bunch length. This expression is evaluated at $\mu = 1.0$ for the non-degenerate rigid dipole and quadrupole cases, when $(m, k) = (1, 0)$ and $(2, 0)$, and then for the degenerate case (long-range wakefields only) where all the radial modes are summed as

$$F_m = \sum_{k=0}^{\infty} F_{mk}. \quad (6.5)$$

The form factors for the degenerate case $m = 1, 2, 3, 4$ are shown in Fig. 6.1, and the results of the three approaches are shown in Table 6.3. The differences are due mostly to the variations in the form factor. For example, the zero growth rates of the non-degenerate analytical approach are at the points where the form factor goes to zero. All of the coupled bunch modes listed in Table 6.3 are unstable, and require either passive or active damping. RHIC will use passive damping to reduce the growth rates to within the damping rate of the wideband system. Based on the above analysis, impedance limits were calculated for the 26 MHz accelerating cavity by setting the growth rate to $2s^{-1}$ and solving for R_{SH} in Eq. 6.3. The form factor used is the greater of the dipole or quadrupole, i.e. at $\chi = 2.9$ it changes from dipole to quadrupole. This growth rate is a factor of 5 below the $10s^{-1}$ damping rate of the wideband longitudinal feedback system.

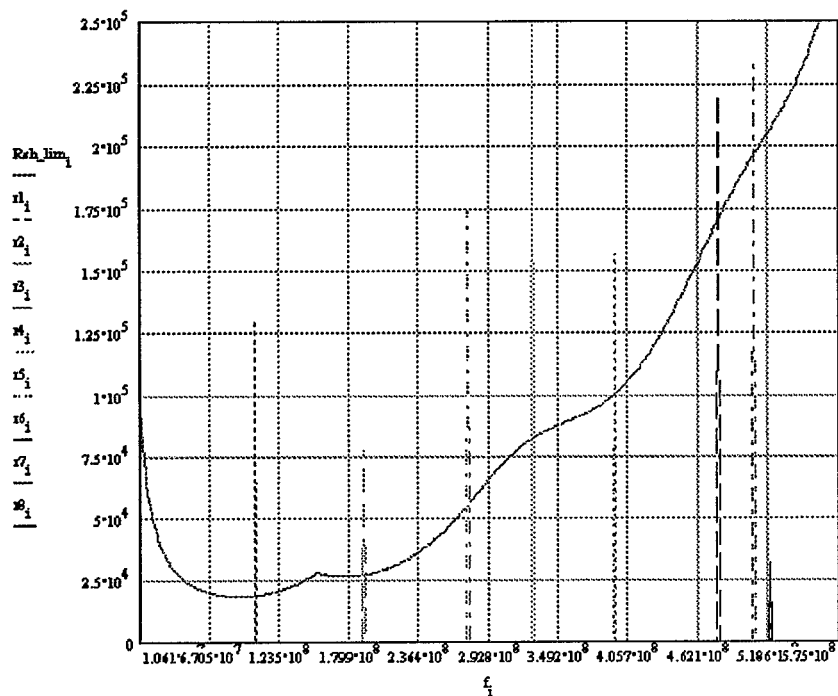


Figure 6.2: Impedance limit for 26.7 MHz accelerating cavity longitudinal modes. Horizontal axis is frequency [Hz], vertical axis is the shunt impedance [Ω].

This impedance limit is shown in Fig. 6.2.

This wideband damper is required for the correction of injection momentum errors (see “Feedback and damping systems”) and has a damping rate of $10s^{-1}$. In addition, the storage cavities could be used to increase the synchrotron frequency spread and hence the Landau damping. The storage cavities have a damping loop which is required at transition crossing, but which could be withdrawn to provide an additional beam induced voltage at 196 MHz for the same desired effect.

The growth rates during storage have been calculated to be $< .4 s^{-1}$ for the worst cases. During storage the bunches fill the 196.1 MHz buckets and the resulting synchrotron frequency spread is estimated to Landau damp the instabilities as calculated by ZAP. It is therefore not necessary to operate the wide band damper system during this part of the cycle, eliminating possible concerns due to low level damper noise.

6.2 Transverse instabilities

This section is concerned with estimating the growth rates of the beam transverse modes. The analysis is limited to dipole fields, as appropriate to a beam filling only a small fraction of the aperture. Coherent betatron oscillations can arise from a number of sources. These oscillations lead to coherent electromagnetic fields which act back upon the bunch, via the transverse impedance. If this feedback loop is unstable, the oscillations may need to be damped by external feedback if the beam is to survive. The three major sources of transverse impedance are space charge, cavity resonances, and the resistive wall effect.

It is not as straightforward to apply transverse instability theory to RHIC as it is to apply longitudinal instability theory. Calculations are easiest in the “weak coupling limit”, when the frequency shift of a mode is small compared to the synchrotron frequency. This is not always the case for RHIC, especially at low energies - at injection and part way up the ramp. On the other hand, calculations which include mode coupling and which are not in the weak coupling limit are not yet fully reliable. At low energies the space charge tune shift is large compared to the synchrotron tune, further complicating mode coupling calculations.

6.2.1 Weak coupling calculations

The space charge impedance can be very large. It is given by

$$Z_{SC}^{\perp}(\omega) = i \frac{RZ_0}{\beta^2 \gamma^2} \left(\frac{1}{a^2} - \frac{1}{b^2} \right), \quad (6.6)$$

where R is the machine radius, $\beta = v/c$, γ is the Lorentz factor, $Z_0 = 377\Omega$, a is the radius of a uniform equivalent beam, and b is the radius of the vacuum chamber. The space charge impedance is not truly independent of frequency ω , but decays exponentially when $\omega \gtrsim \omega_c \gamma \beta$, where ω_c is the cutoff frequency for waveguide modes in the beam pipe. This exponential cutoff is neglected in what follows. Parasitic modes in cavities, and cavity like objects, produce resonator impedances described by Equation 1.16, and parameterized by the transverse shunt impedance R_{sh} , the quality factor Q , and the angular resonant frequency ω_r . Radio frequency cavities are by far the dominant source of transverse resonances in RHIC, as described by Tables 3.2 and 3.5. The resistive wall impedance for RHIC is parameterized by the “two pipe model” of Equation 2.5. The effective resistivity of the beampipe wall material was taken to be $0.72 \mu\Omega\text{m.}$, which is quite large.

Growth rate estimates including all these effects are carried out in the weak coupling limit, for protons and gold, at injection and halfway up the magnetic ramp, using codes like ZAP [32]. Results are shown in Tables 6.4 through 6.7, for various chromaticities with and without active damping. The chromaticity

χ	α_d [s ⁻¹]	α_{\max} [s ⁻¹]	l	s
0.0	0	26.6	0	28
1.4	0	.06	5	28
2.8	0	.00	19	28
0.0	30	.002	5	2
1.4	30	.002	8	28
2.8	30	.000	—	—

Table 6.4: Growth and damping rates for protons at injection.

χ	α_d [s ⁻¹]	α_{\max} [s ⁻¹]	l	s
0.0	0	5.60	0	28
1.4	0	.30	1	28
2.8	0	.08	2	28
0.0	6	.004	3	2
1.4	6	.003	5	28
2.8	6	.005	5	28
4.2	6	.002	6	28

Table 6.5: Growth and damping rates for protons halfway up ramp.

is defined by

$$\chi = p \frac{dQ}{dp}. \quad (6.7)$$

and the damping α_d is provided by the transverse damper acting on rigid bunches. For comparison purposes, note that the feedback system described in Chapter 5 has a maximum damping rate of $\alpha_d \sim 780\text{s}^{-1}$ - a damping time of 100 turns - at injection. The tables show the growth rate α_{\max} of the fastest growing mode, identified by its synchrotron mode number l and its coupled bunch mode number s .

In all cases before storage, transverse instabilities can be controlled with a slight amount of chromaticity, and a modest damping rate in a rigid damping system. Note that the effective resistivity of the beampipe wall material was

χ	α_d [s ⁻¹]	α_{\max} [s ⁻¹]	l	s
0.0	0	20.8	0	28
-1.4	0	7.73	0	28
-2.8	0	1.86	1	28
-4.2	0	.38	2	28
-5.6	0	.07	4	28
0.0	30	.00	6	2
-1.4	30	.00	—	—
-2.8	30	.00	—	—

Table 6.6: Growth and damping rates for gold at injection.

χ	α_d [s ⁻¹]	α_{\max} [s ⁻¹]	l	s
0.0	0	4.40	0	28
1.4	0	.03	3	28
2.8	0	.00	9	28
0.0	6	.00	14	2
1.4	6	.00	17	24
2.8	6	.00	17	28

Table 6.7: Growth and damping rates for gold halfway up ramp.

taken to be $0.72\mu\Omega\text{m}$, which is quite large.

During storage, as through the rest of the cycle, the largest contribution to the impedance is due to transverse space charge effect. This impedance is $8\text{M}\Omega/\text{m}$ and $19\text{M}\Omega/\text{m}$ for protons and gold, respectively. The resulting tune shifts are small compared to the synchrotron tune $Q_s \simeq 5 \times 10^{-3}$. Assuming a smooth distribution in the transverse variables, any coherent motion should be Landau damped as long as the betatron tune spread is at least twice as large as the space charge tune shifts calculated when the tune spread is neglected [35]. Multiplying by a safety margin of a factor of 2 results in a minimum root mean square betatron tune spread of 2×10^{-3} , which is reasonable to expect in practice.

Therefore, the instabilities predicted using the weak coupling formalism are controllable during injection and acceleration, and are Landau damped during storage.

6.2.2 Calculations with mode coupling

For RHIC parameters, the incoherent space charge frequency shift $\Delta\omega_I$ is significantly larger than the synchrotron frequency at injection and partway up the acceleration ramp. The weak coupling limit assumes, to the contrary, that the frequency shift is small compared to the synchrotron frequency. Calculations which include synchrotron mode coupling have therefore been started.

A calculational technique which includes the effects of space charge frequency spread, synchrotron mode coupling, multiple bunch effects, and chromaticity has been developed [36]. A Gaussian unperturbed distribution is assumed. For a given coupled bunch mode s , a maximum synchrotron mode number ℓ_{max} is chosen. Radial and synchrotron modes k and ℓ satisfying $|\ell| + 2k \leq \ell_{\text{max}}$ are included in the calculation. Previous studies [37] indicate that this is a reasonable partitioning of the expansion indices. When space charge is neglected, the results are identical to those obtained using Chin's technique [38] which forms the basis for the MOSES code. These "state of the art" calculational tools are still under active development, and their effectiveness and accuracy are not yet clear.

Calculations have been performed using the new technique, including the space charge tune spread, for comparison with the older technique, which does not include it. A beam model with a constant line density within the bunch (a boxcar) is considered, as well as a Gaussian distribution. There is no longitudinal variation of the space charge tune shift in the boxcar model, which has an exact solution for a pure space charge impedance [39]. For the case of a general impedance, reducing the partial differential equation to a matrix problem is straightforward [36]. The matrix truncates to a finite dimension for a pure space charge impedance so that the expansion is around exact solutions for the dominant impedance. Gaussian and boxcar distributions with identical peak line densities are considered, in order to compare different distributions in

longitudinal stability calculations [40].

Consider injection, which appears to be the most worrisome part of the cycle. The quantity of interest is the growth rate α_{\max} of the most unstable mode. For a normalized 95% emittance of $15\pi\mu\text{m}$, the incoherent space charge tune shifts for protons and gold satisfy $\Delta\omega_I/\omega_s \approx 20$ and $\Delta\omega_I/\omega_s \approx 13$, respectively. Since the frequency shift of the first rigid mode is comparable in magnitude to the space charge frequency shift, one requires $\ell_{\max} \gtrsim 20$ and $\ell_{\max} \gtrsim 13$ for protons and gold, respectively. This is a lot of modes. Calculations for such large values of ℓ_{\max} are very time consuming in the current computational scenario. In an attempt to understand the parameter dependence, calculations are performed for a range of values of $\Delta\omega_I/\omega_s \leq 10$ and $\ell_{\max} \leq 15$.

At the time of writing, this promising calculational technique is not ready for firm predictions. However, development of the technique continues.

6.3 Landau damping in RHIC

The two main sources of Landau damping in RHIC are nonlinearity of the rf restoring force, and nonlinearity of the lattice. While the former leads to an amplitude dependent synchrotron tune $Q_s(A_\delta)$, the latter leads to an amplitude dependent betatron tune $Q(A_\beta)$. The size of the synchrotron tune spread depends on the relative size of the bunch and bucket areas. Gold ion bunches that diffuse through intrabeam scattering during storage eventually fill the rf bucket (and spill out of it), with a consequently large synchrotron tune spread. A significant betatron tune spread is present even at injection, when it is mainly driven by the chromaticity sextupoles, to second order in their strength. At storage it is dominated by IR quadrupole triplet nonlinearities. If necessary, octupole circuits in RHIC can be powered to enhance the betatron tune spread.

Longitudinal instabilities may be stabilized by the synchrotron tune spread. For a longitudinal density of the form

$$\rho(\phi) \propto (\hat{\phi}^2 - \phi^2)^2 \quad (6.8)$$

dipole longitudinal instabilities are damped if the tune shift ΔQ_0 , calculated using a pure quadratic rf potential, satisfies

$$\Delta Q_0 \lesssim Q_s(0) - Q_s(\hat{\phi})/4 \quad (6.9)$$

where $Q_s(r)$ is the synchrotron tune as a function of amplitude in the octupole approximation [41]. For Gaussian bunches the stability criterion becomes [42]

$$\Delta Q_0 \lesssim Q_s(0) - Q_s(\sigma)/2 \quad (6.10)$$

For nearly full buckets the octupole approximation breaks down and a more careful analysis is needed. Quadrupole and higher order mode longitudinal oscillations are usually stable if the dipole modes are stable.

Transverse instabilities are stabilized by both sorts of tune spread. A formalism which incorporates betatron tune spread in Gaussian bunches has been developed by Chin [43]. This technique neglects space charge tune spread and appears fairly difficult in practice. An alternative technique which seems to have reasonable numerical properties has also been developed, but RHIC specific results have not been obtained [36]. Nonetheless, a crude rule of thumb is that coherent motion is Landau damped if the betatron tune spread in a bunch is larger than two times the space charge tune shifts. As already discussed above, this means that even modest rms betatron tune spreads of about 2×10^{-3} are very effective in practice.

6.4 The head-tail instability

The head-tail instability couples the longitudinal and transverse motion of a single bunch together with potentially disastrous consequences[8]. If the head of a bunch is assumed to be infinitesimally displaced transversely, then it can drive the motion of the tail of the bunch. Half of a synchrotron period later, the positions of the head and the tail are reversed, and the enhanced oscillation of what is now the head of the bunch can drive the tail of the bunch even further. It is easy to make a crude two particle linear matrix model of this situation, and to make the corresponding two particle simulation. This leads to a condition for “strong head-tail” stability that does not depend on the chromaticity at all. However, although practically all electron and hadron storage rings observe the head-tail effect, it is universally found to depend strongly on the horizontal and vertical chromaticities.

A more realistic model of the “head-tail” effect (without the “strong” adjective) incorporates the chromaticity dependent betatron phase shift that the tail undergoes while moving to the head of the bunch. The stability criterion derived from this model includes the chromaticity, and is in semiquantitative agreement with observation. Crudely speaking, both chromaticities should be a few units negative below transition, and a few units positive after transition. This is sufficient to ensure head-tail stability in all existing storage rings. It is assumed to also be sufficient for RHIC, where the chromaticity is nominally $\chi \simeq -3$ below transition, and $\chi \simeq +2$ above transition. This leads to the dynamical question of how fast the chromaticity must be reversed while crossing transition, and to the engineering question of whether or not RHIC sextupoles have a fast enough slew rate.

A conservative approach is to require the chromaticity reversal to be done in one synchrotron oscillation period, about 28 ms just before and just after transition[5]. (The use of a transition jump ensures that the synchrotron frequency does not get arbitrarily close to zero.) This is conservative because it allows only about one iteration for the head-tail instability to build up to an unacceptable level. Realistic head-tail blow up times are many synchrotron

periods long, and many blow up times must pass before an infinitesimal disturbance becomes significant. Nonetheless, the sextupole slew rate in RHIC is adequate to meet even the conservative criterion with a 5 unit chromaticity shift calculated to take ~ 30 ms.

Chapter 7

Summary and Comments

The RHIC narrowband impedance spectrum is dominated by rf cavities. The resonances from the 26 MHz cavities used during injection are somewhat stronger than those from the 200 MHz cavities used during storage.

The RHIC broadband impedance spectrum is dominated by the resistive wall effect at very low frequencies and by kicker magnets in the intermediate frequency range up to 3 GHz. In this report we extrapolate the effect of the abort kickers (7 modules per ring) from preliminary measurements of the injection kicker prototype module (4 per ring) with no beam pipe. The abort kicker modules are conservatively assumed to give the same size contribution to the total impedance, although the real contribution will be less, because their aperture is larger. We are actively pursuing the use of image current strips on the outside of the ceramic beam pipes to reduce the impedance of these elements.

The threshold for longitudinal microwave instabilities is lowest for protons during rebucketing, with a $|Z^{\parallel}/n|$ broadband impedance limit of 2.1Ω in the frequency range 400 MHz to 3 GHz. If we limit the longitudinal emittance growth for gold ions at transition to about 10%, the broadband impedance limit then becomes 1.5Ω , almost three times the total estimated impedance for the ring at the relevant bunch frequencies of 400 MHz and above.

Longitudinal coupled bunch growth rates are worst for protons at injection. Calculations show that the passive higher order mode dampers on the 26 MHz cavities will limit the worst case growth rate to 2 s^{-2} , well within the range of the active longitudinal damping system that will have a maximum damping rate of 10 s^{-1} . At storage the 200 MHz cavities will give a worst case growth rate of less than 1 s^{-1} , well within the parameters of the active damping system, if not Landau damped.

Transverse coupled bunch growth rates are also worst for protons at injection, when the resistive wall impedance may lead to a growth rate of about 26 s^{-1} . The transverse damper system is designed to handle growth rates up to 720 s^{-1} and so will easily stabilize any emittance growth from the resistive wall

instability at injection and during acceleration. At storage the beams will be Landau damped. Calculations performed in the weak coupling limit show that the stored beam is stabilized against transverse coupled bunch instabilities by adjusting the chromaticity.

Space charge is a very significant effect, since it places a limit on the longitudinal impedance for gold ions at transition. Space charge also produces a tune spread that can be much larger than the synchrotron tune, especially at injection energies. Calculations of mode coupling instabilities in this regime are less reliable than in the traditional weak coupling regime. We will continue to develop the strong coupling model and to compare our results with other machines.

All species of ion beams are expected to be stable during storage. At lower energies the damping systems and chromaticity corrections will limit any growth to acceptable levels during the short time it takes to get from injection to storage.

Bibliography

- [1] "Workshop on the RHIC Performance", Eds. F. Khiari, J. Milutinovic, A. Ratti, and M. J. Rhoades-Brown, BNL-41604, 1988.
- [2] J. Wei, "Evolution of a Hadron Beam Under IBS", p3651, Proc. of PAC 93, Washington, 1993.
- [3] "The Conceptual Design of the RHIC RF System", RHIC/RF note, BNL, May 1993.
- [4] "RHIC Design Manual", August 1993.
- [5] J. Wei, S. Peggs, "Transition Crossing in the RHIC", BNL-45923 AD/RHIC-84, 1984.
- [6] J. Wei, "Transition-Energy Crossing with a γ_t -Jump", Proc. of EPAC 94, London, 1994.
- [7] S. Peggs, S. Tepikian, D. Trbojevic, p168, Proc. of PAC 93, Washington, 1993.
- [8] A. Chao, "Physics of Collective Beam Instabilities in High Energy Accelerators", John Wiley & Sons, 1993.
- [9] A. Chao, SLAC-PUB-2946, June 1982.
- [10] T. Weiland, Particle Accelerators 15 (1984), pp. 245-292, 1984.
- [11] S. Peggs et al, "An Impedance Model of the Relativistic Heavy Ion Collider, RHIC", Proc. EPAC 94, London, 1994.
- [12] J. Rose, "Calculations of HOMs and Coupled Bunch Instabilities due to the RHIC rf Cavities", Proc. of EPAC 94, London, 1994.
- [13] H. Hahn, S. Tepikian, Proc. of PAC 91, p.1707, 1991.
- [14] K. Bane, SLAC-PUB-4618, May 1988.
- [15] V. Mane, S. Peggs, RHIC/AP/26, BNL, May 1994.

- [16] V. Mane, RHIC/AP/15, BNL, November 1993.
- [17] V. Mane, RHIC/AP/7, BNL, August 1993.
- [18] V. K. Neil, A. M. Sessler, Rev. Sci. Instr., 36, pp.429, 1965.
- [19] L. J. Laslett, Proc. Int. Symp. on Electron and Proton Storage Rings, Saclay (1966), IV-5, 1966.
- [20] E. B. Forsyth, "RHIC Injection Kicker", unpublished, December 1992.
- [21] G. Nassibian, CERN/PS 84-25 (BR), 1984.
- [22] S. Kurennoy, Proc. PAC 93, p. 3420, Washington, 1993.
- [23] V. Mane, S. Peggs, "Pump-out port impedance", RHIC/AP/34, July 1994.
- [24] V. Rodel, "Higher-order modes and tuning of the SPS 200 MHz single-cell cavity", CERN SL/RFS/91-08, 1991.
- [25] K. Halbach and R. F. Holsinger, "SUPERFISH - A Computer Program for Evaluation of RF Cavities with Cylindrical Symmetry", Particle Accelerators 7, 213 (1976).
- [26] J. Tuckmantel, "Application of SAP in URMEL", CERN-EF/RF 83-5, 83-4 CERN, Geneva, Switzerland, 1983.
- [27] J. Rose et al, "Conceptual design of the 26.7 MHz rf System for RHIC", Proc. PAC 93, Washington, 1993.
- [28] F. Caspers, G. Dome, H.P. Kinderman "A New Type of Broadband Higher Order Mode Coupler Using Parallel Ridged Waveguide in Comparison with a Coaxial Filter Version", Proc. PAC 87, Washington, 1987.
- [29] SYBASE Inc., 6475 Christie Avenue, Emeryville, CA, 94608.
- [30] A. Hoffman, "Single-Beam Collective Phenomena — Longitudinal", CERN 77-13, 1977.
- [31] J.M. Wang and C. Pellegrini, "On the Condition for a Single Bunch High Frequency Fast Blow-Up", Proc. 11th Inter. Conf. High-Energy Accel. (Geneva, 1980), p.554.
- [32] M. Zisman, S. Chattopadhyay, J.J. Bisognano, "ZAP User's Manual", LBL-21270 UC-28 December, 1986.
- [33] R. Baartman, "Effect of the Beam on RF", US Particle Accelerator School, Florida State University, January 1992.
- [34] K. Satoh, SLAC PEP note 357, 1981.

- [35] See, for example, the ZAP manual, page 153.
- [36] M. Blaskiewicz and W. T. Weng, "Effect of Space Charge Tune Shift on Transverse Instabilities", Proc. EPAC 94, London, 1994. Also to be published in Phys. Rev. E.
- [37] R. Kohaupt, DESY 80-22, Hamburg, 1980.
- [38] Y.H. Chin, CERN SPS/85-2, Geneva, 1985.
- [39] For example, see F. Sacherer, CERN/SI-BR/72-5, Geneva, 1972.
- [40] R. Baartman and E. N. Shaposhnikova, TRI-DN-91-K168), Vancouver, 1991.
- [41] M. Blaskiewicz, Proc. PAC 93, p. 3324, Washington, 1993.
- [42] B. Zotter, CERN SPS/81-19 (DI), Geneva, 1981.
- [43] Y.H. Chin, CERN SPS/85-9 (DI-MST), Geneva, 1985.